High-Density Ceramics Obtained By Andesite Basalt Sintering

Vladimir Pavkov (pavkow@vin.bg.ac.rs)
VINCA Institute of Nuclear Sciences: Univerzitet u Beogradu Institut za nuklearne nauke Vinca
https://orcid.org/0000-0002-9799-8713

Gordana Bakić
University of Belgrade Faculty of Mechanical Engineering: Univerziteta u Beogradu Fakultet Masinski

Vesna Maksimović
VINCA Institute of Nuclear Sciences: Univerzitet u Beogradu Institut za nuklearne nauke Vinca

Ivana Cvijović-Alagić
VINCA Institute of Nuclear Sciences: Univerzitet u Beogradu Institut za nuklearne nauke Vinca

Marija Prekajski Đorđević
VINCA Institute of Nuclear Sciences: Univerzitet u Beogradu Institut za nuklearne nauke Vinca

Dušan Bučevac
VINCA Institute of Nuclear Sciences: Univerzitet u Beogradu Institut za nuklearne nauke Vinca

Branko Matović
VINCA Institute of Nuclear Sciences: Univerzitet u Beogradu Institut za nuklearne nauke Vinca

Research Article

Keywords: Andesite basalt, High-density ceramics, Cold isostatic pressing, Hardness, Fracture Toughness

Posted Date: August 25th, 2021

DOI: https://doi.org/10.21203/rs.3.rs-827727/v1

Abstract

Modern industrial requirements include not only the usage of constructive materials with good mechanical properties but also materials obtained through environmentally friendly and low-cost processing procedures. Basalt, as a low-cost raw material, is regarded as a good candidate for industrial constructive parts production. In the present study, andesite basalt originated from the deposit site "Donje Jarinje", Serbia, was examined as a potential raw material for high-density ceramics production. The production of high-density ceramics included dry milling, homogenization, cold isostatic pressing, and sintering in the air. To determine the optimal processing parameters the sintering was conducted at 1040, 1050, 1060, 1070, and 1080 °C, and afterward the sintering duration was varied from 30 to 240 min at the optimal sintering temperature of 1060 °C. Characterization of the starting and sintered materials included the estimation of particle size distribution, density, hardness, and fracture toughness complemented with X-ray diffraction, light optical microscopy, scanning electron microscopy, and energy dispersive spectroscopy analysis. Phase transformations did not occur during processing in the investigated temperature range from 1040 to 1080 °C. The obtained research results showed that 99.5% of relative density and the highest hardness and fracture toughness values of 6.7 GPa and 2.2 MPaÖm, respectively, were achieved for the andesite basalt sintered at 1060 °C for 60 min in the air. The results of the presented study confirmed that the sintered andesite basalt can be used as a high-density ceramic material for various industrial applications since this environmentally friendly material shows satisfactory mechanical properties.

Introduction

In modern industrial practice, environmentally friendly and lightweight constructive materials with good mechanical properties, produced from low-cost abundant materials, are highly demanded. Basalt is a natural material that meets all of these criteria. Namely, basalt is a natural igneous rock of volcanic origin, which covers about 70% of the Earth’s crust [1]. As a result of the rapid cooling of lava on the Earth's surface, basalt is usually present in fine-grained condition and belongs to the group of grey-to-black colored and extremely hard rocks. The technology of basalt rock processing is entirely eco-friendly, which is extremely important for the modern age economy, ecology, and energy-efficiency.

Basalt can be used in the production of heat- and fire-resistant refractory materials owing to its low thermal conductivity, high oxidation resistance, and high softening and melting temperatures [2]. Because of the high chemical durability and high resistance to abrasion and corrosion [3–5], natural basalts are regarded as good replacements for wear-resistant steels and can be used for the production of constructive elements which are during their exploitation exposed to abrasion and corrosive-abrasive wear [6].

Since basalt shows no toxic, carcinogenic, mutagenic, or teratogenic effects [6] it is in a real sense non-hazardous material [7].

High strength, hardness, and toughness [8], low viscosity [9], high corrosion resistance, minimal moisture absorption, ability to withstand high temperatures, thermal insulation, and sound absorption properties [10, 11], high abrasion resistance, exceptional compressive strength, and chemical resistance resulted in the usage of basalt-based products in various industrial applications from civil and mechanical engineering, agriculture, construction industry, and mining, to transportation industry, metallurgy [12–17], and as a decorative material [16, 18].

Moreover, basalts can be used as raw materials for the obtainment of iron-rich glass and glass-ceramic materials [19–24] due to their chemical composition since these volcanic rocks are mainly composed of silica, alumina, iron oxide, calcium, and magnesia with lower content of potassium, titania, manganese, and phosphorus oxide [14]. Classification of basalt rocks is conducted according to the SiO_2 content present in their composition and thus basalts can be classified as alkaline (up to 42% SiO_2), mildly acidic (43–46% SiO_2), and acidic (over 46% SiO_2) [25].

Even though basalt shows numerous advantages for application in diverse industrial areas it is still mostly used in civil engineering, while research data regarding their wider applicability is scarce in the available literature. For this reason, the aim of the presented research was to define the optimal technological processing procedure for the obtainment of low-cost high-density ceramics based on basalt with advanced characteristics and to evaluate their potential industrial applications as environmentally friendly materials.

Experimental Procedure

2.1. Materials and synthesis

Crushed basalt aggregates 2 to 5 mm in size, supplied from the deposit site "Donje Jarinje", Serbia, were used as a starting material for the presented research, Fig. 1. Basalt from this deposit site is distinctly black colored and textured, classified as the andesite basalt [6, 17], also mentioned in the literature as the basaltic andesite [26].

The chemical composition of the andesite basalt used in this study was analyzed utilizing the Oxford INCA 350 Energy Dispersive X-ray (EDX) microanalysis system, Oxford Instruments, UK, coupled with the JEOL JSM-6610LV scanning electron microscope (SEM), JEOL, Japan. For this purpose, five andesite basalt samples were examined and obtained results are summarized in Table 1. Obtained results indicate that the determined chemical composition is characteristic for the andesite basalt rock, *i.e.* content of silica and alumina oxides as predominating compounds in the rock composition is approximately 77 wt.%. Based on the determined SiO_2 content of approximately 58 wt.% the basalt rock, used in this study, can be classified as acidic, Table 1.

Table 1
The chemical composition of the andesite basalt originated from the "Donje Jarinje" deposit site (wt.%).

Compounds	Chemical composition (wt.%)				
	Sample No.				
	1	2	3	4	5
SiO_2	58.21	57.76	59.98	58.97	58.21
Al_2O_3	18.97	19.96	18.34	19.27	18.19
FeO	6.66	5.54	7.36	6.19	7.08
CaO	5.63	7.14	6.91	6.45	7.68
Na_2O	3.94	3.40	2.68	2.47	2.25
MgO	2.86	3.32	1.50	3.57	3.51
K_2O	2.79	2.24	2.61	2.19	2.18
TiO_2	0.95	0.65	0.62	0.87	0.89
Total	100.00	100.00	100.00	100.00	100.00

Andesite basalt was milled in a tungsten-carbide vibrating cup mill Fritsch Pulverisette 9, Germany, for 30 min in a dry state at 800 rpm to obtain the fine powder suitable for synthesis. The obtained powder was mixed with 0.6 wt.% of commercial paraffin wax binder for 10 min in a ceramic mortar. After homogenization, the powder mixture is preloaded under a cold uniaxial pressure of 50 MPa to obtain cylindrical green compacts 12 mm in diameter and afterward subjected to the cold isostatic pressing (CIP) under a pressure of 230 MPa for 2 min to increase the green compacts density. To remove the binder, organic impurities, moisture, and chemically bonded water the green compacts were slowly heated up in the air to 100°C at the heating rate of 1°C/min and held at this temperature for 60 min, and then additionally heated up at the same rate to 650°C and held for 60 min. After binder removal, the basalt-based compacts were heated to the chosen sintering temperature at the heating rate of 5°C/min.

The basalt-based compacts were sintered in the air in the laboratory high-temperature electric resistance box furnace Elektron VTP-03, Serbia, for 60 min at 1040, 1050, 1060, 1070, and 1080°C to determine the optimal sintering temperature necessary for the attainment of the ceramic materials with the highest density. The sintering temperature was constantly monitored and electronically regulated within the maximal temperature deviation of ± 2°C. The cooling rate from sintering to room temperature was 5°C/min. After determining the optimal sintering temperature additional group of samples was sintered at this optimal temperature for 30, 60, 120, 180, and 240 min to obtain the optimal sintering duration.

2.2. Materials characterization

The laser particle size analyzer Mastersizer 2000, Malvern Instruments Ltd., UK, was utilized to determine the particle size distribution of milled andesite basalt powder. The theoretical density (TD) of andesite basalt powder was attained using a pycnometer, distilled water, and analytical balance KERN PFB, Germany, with an accuracy of ±0.01 g. The density of sintered ceramic samples was determined by employing Archimedes' principle using distilled water as the immersion liquid. The relative density of obtained ceramics was calculated based on the obtained theoretical density value. All density measurements were conducted for 5 samples and showed excellent reproducibility.

The phase analysis of milled andesite basalt powder and sintered ceramic samples was conducted by using X-ray diffractometer (XRD) Rigaku Ultima IV, Japan, with filtered Cu$K\alpha_1$ radiation (λ = 0.154178 nm). The X-ray diffraction data were collected over the 2θ range from 3° up to 70° with the step of 0.02° and scanning rate of 5°/min. The PDXL2 v2.0.3.0 software with reference to the diffraction patterns available in the International Center for Diffraction Data (ICDD) was used for the phase identification and data analysis.

To examine the microstructural and morphological characteristics of the sintered ceramic samples these samples were ceramographic prepared using the standard preparation method that included grinding with SiC abrasive papers up to 1000 grit and polishing using 1 μm diamond paste. The microstructure of sintered samples was investigated by a light optical microscope (LOM) Zeiss Axioplan LM, Zeiss, Germany. Morphological characterization of the andesite basalt powder and ceramic sintered samples was performed using an SEM Tescan VEGA TS 5130 MM, Tescan, Czech Republic.

The sintered samples hardness and fracture toughness were determined utilizing the Vickers indentation hardness tester model Buehler Identamet 1114, Buehler, Germany, by applying a load of 3 kgf (29.421 N). All Vickers hardness measurements were conducted at 5 measuring points of each sample with excellent reproducibility. The Vickers hardness (HV_3 [GPa]) was calculated according to Eq. (1) [27]:

$$HV = 1.854 \cdot 10^{-9} \cdot \frac{P}{d^2} \quad (1)$$

where P is an indentation load [N], while d [m] is an average length of the diagonals of the Vickers indentation. The half-penny crack model [28] was used for the calculation of fracture toughness in brittle materials according to Eq. (2):

$$K_{IC} = 0.0752 \cdot \frac{P}{c^{\frac{3}{2}}} \quad (2)$$

where K_{IC} is the fracture toughness [MPa$\sqrt{}$m], P is the indentation load [N], while c is the measured crack length [m]. If a [m] is the half-diameter of the indented section and $c/a \geq 2$ then the crack model can be considered as a half-penny model, while if $c/a < 2$ then the crack model is considered as Palmqvist model [29, 30]. The general assumption is that cracks in brittle materials, characterized with relatively low

toughness, are following the half-penny model and that cracks attained in materials with relatively high toughness can be considered to emulate the Palmquist model [31].

Results And Discussion

3.1. Powder theoretical density

The theoretical density of the milled andesite basalt powder was determined to be 2.63 g/cm^3. The theoretical density value obtained in this study is in good agreement with the available literature data. Namely, the theoretical density of the andesite basalt originated from the "Donje Jarinje" deposit site was estimated to be in the range from 2.60 to 2.63 g/cm^3 [6, 17].

3.2. Powder particle size distribution and morphology

The particle size distribution of the andesite basal powder obtained by milling of the basalt rock is shown in Fig. 2. As can be seen, the values obtained during the powder analysis can be summarized as follows: d(0.1) = 0.465 μm, d(0.5) = 1.917 μm, d(0.9) = 11.803 μm. Bimodal distribution of the powder particles size is evident in the range from 0.2 to 12 μm and from 100 to 300 μm. The volume fraction of powder particles with dimensions ranging from 0.2 to 12 μm is determined to be 93.3%, while the volume fraction of powder particles with dimensions ranging from 100 to 300 μm is estimated to be 6.7%. The observed bimodal particle size distribution enables good powder compaction with the usage of a minimal amount of binder.

The morphology of the andesite basalt powder obtained by dry milling for 30 min is presented in Fig. 3. The presence of angularly shaped particles with a rough surface is clearly visible in the SEM micrograph. Moreover, agglomeration of small powder particles of approximately 0.5 μm in size can also be observed in Fig. 3.

3.3. Relative density

A macrographic overview of the ceramic samples obtained after sintering of the andesite basalt powder compacts in the temperature range from 1040 to 1080°C and in the sintering time range from 30 to 240 min is given in Fig. 4. It can be observed that the initial black color of the andesite basalt rock is transformed after milling into the grey color of the obtained basalt powder which is additionally transformed during sintering in the air to the reddish-brown color of the ceramic samples. The observed color change is induced by the chemical composition alterations, *i.e.* the transition of FeO into Fe_2O_3 according to the following Eq. (3):

$$4FeO + O_2 = 3Fe_2O_3 \quad (3)$$

The final surfaces of the sintered samples under an oxidizing atmosphere are reddish-brown color suggesting the presence of Fe^{3+} ions and the formation of hematite (Fe_2O_3) [32–36].

Based on Fig. 4 it can be seen that with an increase of the sintering temperature a change in the reddish-brown color from lighter to darker shades of the sintered ceramic samples occurs. The significant color change is clearly visible when the sintering temperature was increased from 1040 to 1050°C. However, it must be underlined that the research results indicated that the observed color alterations do not influence the quality of the obtained ceramic samples.

The effect of sintering temperature on density of ceramic samples obtained after 60 min long sintering of the andesite basalt powder is presented in Fig. 5. As can be seen, the lowest relative density of 92.9% was measured in ceramic samples sintered at 1040°C. The relative density of the obtained ceramics increases with an increase in sintering temperature reaching the maximum value of 99.5% in sample sintered at 1060°C. Therefore, this temperature will be designated as optimal. Based on the available literature data [17, 36, 37] and results obtained in the present study, this is the highest relative density achieved during basalt sintering. As the sintering temperature further increases, the relative density of the obtained ceramic samples decreases. Namely, at sintering temperatures of 1080°C the relative density of 95.8% is achieved. Research results presented in Fig. 5 show that small sintering temperature alterations have a significant impact on relative density.

The decrease in density of samples sintered above 1060°C can be explained with the help of "liquid channels". In the localized surface area of the ceramic samples sintered at 1070 and 1080°C the appearance of so-called "liquid channels" was noticed. The similar phenomenon was observed at the andesite basalt surface originated from the same locality [17]. This phenomenon was also reported for the olivine basalt and explained with the occurrence of partial melting of formed crystal phases between the solidus and liquidus temperatures [37]. Moreover, previous research in this field showed that a higher silicon, sodium, and potassium contents in the basalt composition led to an increase of the glassy phase content in the microstructure, which reduced the material density and increased its acid resistance [38].

Polished surfaces of ceramic samples sintered at 1040, 1060, and 1080°C for 60 min are presented in Fig. 6. Shown LOM micrographs demonstrate that the reason for a decrease in the relative density of samples sintered above 1060°C is the appearance of surface craters as a result of melting and evaporation of the material, Fig. 6c. The size of the observed surface craters is up to 50 μm.

The effect of sintering time on the density of ceramic samples sintered at 1060°C is presented in Fig. 7. A decrease of the sintering duration from 60 min to 30 min, as well as an increase of the sintering time to 120, 180, and 240 min, did not lead to an increase of relative density. Namely, obtained results indicated that the relative density of the sintered samples decreased with an increase in the sintering duration. Therefore, the optimal sintering temperature and time were found to be 1060°C and 60 min, respectively.

3.4. Shrinkage

The effect of sintering parameters on the shrinkage of high-density ceramic samples is presented in Fig. 8. The effect of sintering temperature on shrinkage is given in Fig. 8a which shows that the shrinkage increases with an increase in sintering temperature, reaching the maximum value of 12.81% in samples

sintered at 1060°C. Further increase in sintering temperature causes a decrease of shrinkage reaching the value of 10.83% in samples sintered at 1080°C.

The difference between the maximum and minimum shrinkage value of 1.98% was observed during the sintering in the specified temperature range. If compare graphs given in Fig. 5 and Fig. 8a one can conclude that the effect of sintering temperature on relative density and shrinkage is quite similar. This is expecting knowing that the increase of relative density as well as the increase of shrinkage is affected by pore elimination.

The effect of sintering time on the shrinkage of high-density ceramic samples sintered at 1060°C is presented in Fig. 8b. It is evident that a decrease in sintering time to 30 min, as well as an increase in sintering time to 120, 180, and 240 min, did not contribute to an increase of the shrinkage. The lowest shrinkage of 12.12% was measured in samples sintered for 240 min. The negligible difference of only 0.69% between the maximum and minimum shrinkage value could be detected at the optimal sintering temperature.

3.5. Weight loss during sintering

The effect of sintering parameters on the weight loss of the obtained high-density ceramic samples is presented in Fig. 9. From the research results presented in Fig. 9a, it can be observed that the highest weight loss of 3.10 wt.% was detected during sintering at 1080°C, while the lowest weight loss of 2.81 wt.% was measured after sintering at 1050°C. The slight difference between the maximum and minimum weight loss value of 0.29 wt.% was observed during the high-density ceramics sintering in the specified temperature range, although the detected weight loss was increased with an increase of the sintering temperature to 1080°C.

The effect of sintering duration on the weight loss of high-density ceramic samples attained during sintering of the andesite basalt powder at 1060°C is presented in Fig. 9b. Presented research results indicate that in the sintering time range from 30 to 240 min during the processing at the optimal sintering temperature the highest weight loss of 3.01 wt.% was evident after sintering for 30 min, while the lowest weight loss of 2.87 wt.% was shown for the ceramic samples sintered for 120 min. Namely, the negligible difference of only 0.14 wt.% between the maximum and minimum weight loss value could be detected after the high-density ceramics sintering at the optimal sintering temperature.

It must be emphasized that the weight loss in the range from 3.19 to 3.77 wt.% was also recorded during the sintering of the basalt originated from the Arkhangelsk region in Russia where the detected weight change variation was confirmed to be within 0.60 wt.% range [38]. Having this in mind it can be concluded that the lower weight loss was recorded during the sintering in the air of the andesite basalt originated from the deposit site "Donje Jarinje", which was used in this study, then during the sintering of the basalt from the deposit site located in the Arkhangelsk region, which was reported in the literature. Previously published research results indicate that during the basalt heat treatment the weight loss can be expected due to the hygroscopic moisture evaporation, the chemically bound water removal, burnout

of the organic impurities, dissociation of the present carbonates and sulfides, and removal of the gaseous inclusions [36, 38]. Therefore, it can be presumed that the andesite basalt from the "Donje Jarinje" deposit site shows higher purity and can be considered as a high-quality raw material for the high-density ceramics production.

3.6. Phase composition

Phase analysis of the starting andesite basalt material was performed using X-ray powder diffraction analysis to reveal its main mineralogical composition. For that purpose, the andesite basalt rock was crushed and milled into fine powder form. The obtained andesite basalt mineralogical composition is presented in Fig. 10. Based on the shown XRD pattern andesine, as an intermediate member of plagioclase mineral series ($(Na,Ca)Al(Si,Al)Si_2O_8$), was identified as a dominant mineral of the basalt rock used for the presented research. Moreover, labradorite ($(Ca,Na)Al(Al,Si)Si_2O_8$), as another mineral from the plagioclase series which is richer in Ca than andesine, was also identified. Furthermore, small amounts of other minerals, such as olivine $(Mg,Fe)_2SiO_4$) and magnetite (Fe_3O_4), as well as the common rock-forming pyroxene minerals, such as augite ($(Ca,Na)(Mg,Fe,Al,Ti)(Si,Al)_2O_6$) and clinohyperstene ($(Mg,Fe)SiO_3$), were additionally identified in the basalt rock sample.

XRD patterns of all sintered high-density ceramic samples obtained during the present study along with starting andensite basalt powder are presented in Fig. 11. Since the sintered ceramic samples are pressed in the form of a pastille they had to be placed in a sample holder for the solid sample analysis. This holder is made of polyethylene terephthalate glycol (PETG) by using the Ender-5 3D printer, Creality, China. Due to the usage of the PETG sample holder small intensity hump (broad peak) in the low angle region (2θ range from 10° to 20°) can be observed on the recorded XRD patterns, indicating the presence of amorphous phase ascribed to PETG.

Detail analysis of the obtained XRD patterns, given in Fig. 11, shows that there is no significant difference between the recorded diffractograms of the ceramic samples sintered under different conditions indicating the absence of the phase transformations during these treatments. The only difference that can be singled out is the presence of hematite (Fe_2O_3) in the patterns of the high-density ceramic samples which is absent in the XRD pattern of the starting andesite basalt powder. The appearance of hematite during sintering in the air was expected (please see Eq. 3) and the assumption on the transition from FeO to Fe_2O_3, which was made based on the coloration of the sintered samples, is in this way confirmed.

3.7. Hardness

SEM micrograph of the polished surface of high-density ceramic sample obtained during sintering at 1060°C for 60 min is given in Fig. 12. Isolated closed spherically-shaped pores, with dimensions up to 2 μm, are visible after sintering under these optimized conditions (Fig. 12) in contrast to the distinctly irregularly-shaped pores with mostly negative curvatures and a large surface-to-volume ratio present in the ceramic sample obtained during sintering at 1040°C for 60 min (Fig. 6a). Namely, it can be concluded

that with an increase of the sintering temperature the pores inevitably present in the ceramic structure will tend to change their shape, *i.e.* pores will tend toward cylindrical to spherical morphologies and positive curvature with the lowest surface-to-volume ratio, clearly visible in Fig. 12. SEM micrograph, shown in Fig. 12, also indicates the non-homogenous structure of the ceramic sample obtained during sintering at 1060°C for 60 min in the presence of different aggregates and a clear boundary in between.

The effect of sintering temperature on the hardness of ceramic samples attained during sintering of the andesite basalt powder for 60 min is presented in Fig. 13a. A minimal hardness value of 4.8 GPa was achieved at an initial sintering temperature of 1040°C. As the sintering temperature increases, the hardness increases and reaches a maximal value of 6.7 GPa during sintering at 1060°C. With a further increase in the sintering temperature, the hardness value begins slightly to decrease and for the ceramic sample obtained at 1080°C the hardness value reaches 6.1 GPa. By comparing the obtained density values (Fig. 5) and the measured hardness values (Fig. 13a) the expected conclusion that the hardness correlates with the density of the sintered samples can be drawn and accordingly with an increase of the sample relative density its hardness increases.

The effect of sintering time on the hardness of ceramic samples attained during sintering of the andesite basalt powder at 1060°C is presented in Fig. 13b. It is clear from Fig. 13b that a decrease in sintering time to 30 min, as well as an increase in sintering time to 120, 180, and 240 min, did not contribute to an increase of the hardness value. Namely, when the sintering duration increases from 60 to 240 min then the hardness decreases linearly due to a decrease in the sintered ceramic samples density. The maximal hardness value of 6.7 GPa was attained at the optimal sintering temperature during sintering for 60 min.

3.8. Fracture toughness

The effect of sintering temperature on the fracture toughness of ceramic samples attained during sintering of the andesite basalt powder for 60 min is presented in Fig. 14a. Results obtained during the present study show that the fracture toughness value remains unchanged when the sintering temperature is increased from 1040 to 1060 °C and reaches a value of 2.2 MPa$\sqrt{m}$. However, a further increase of the sintering temperature to 1070 and 1080 °C induced a decrease of the fracture toughness to 1.8 MPa$\sqrt{m}$.

The effect of sintering time on the fracture toughness of ceramic samples attained during sintering of the andesite basalt powder at 1060 °C is shown in Fig. 14b. Presented results show that at the optimal sintering temperature the fracture toughness values vary only slightly in the narrow range from 2.0 to 2.2 MPa$\sqrt{m}$ even though the sintering duration is changed during the experiments by 5 times (from 30 to 240 min). The maximal fracture toughness value of 2.2 MPa$\sqrt{m}$ was reached after sintering for 60 min, while the minimum value of 2.0 MPa$\sqrt{m}$ was reached after sintering for 240 min. From the results presented in Fig. 14b it is clear that a longer sintering time at the optimal sintering temperature of 1060 °C did not contribute to an increase in the fracture toughness, although this could be expected as this is the case with most ceramic materials.

Figure 15 shows the impression of a square-based diamond pyramid made at the surface of the high-density ceramic sample sintered under the optimal sintering conditions, *i.e.* at 1060 °C for 60 min, for which the highest relative density of 99.5% was obtained and cracks created at the corners of the impression made during the Vickers test method. It can be seen that the crack propagation is radial relative to the axis of the imprint and that formed cracks have not branched out into many smaller cracks.

If the maximal fracture toughness value of 2.20 MPa√m, obtained during this study, is compared with the fracture toughness values of some aluminosilicate rocks, such as granite (granite fracture toughness value is ranging from 0.97 to 1.15 MPa√m) [39], it can be concluded that during this study the optimization of the sintering procedure led to fabrication of the refractory high-density ceramics with the fracture toughness value two times higher than granite.

Conclusions

Raised public awareness on the usage of green technological solutions in the industrial practice focused the presented research on the development of low-cost procedures for the obtainment of high-density ceramics with multiple applicability using the abundant environmentally-friendly raw materials, such as andesite basalt. The present research was aimed at the obtainment and optimization of the technological process for the production of refractory high-density ceramics using the andesite basalt from the deposit site "Donje Jarinje", Serbia, as the starting raw material and resulting conclusions are summarized as follows:

1. Sintering in the air was successfully applied to obtain the high-density ceramics by using the andesite basalt rock as a low-cost raw material. Relative density of 99.5% was achieved for the ceramic samples produced through the optimized technological process that included the obtainment of bimodal andesite basalt powder and sintering at 1060 °C for 60 min. Application of these optimized sintering parameters ensured the attainment of the basalt-based ceramics with the highest relative density compared to the results available in the relevant literature.

2. The highest shrinkage of 12.81% was achieved for high-density ceramics during the sintering at an optimal temperature of 1060 °C for 60 min.

3. During sintering in the air, no significant loss of material was detected.

4. XRD analysis showed that phase transformations did not occur during the andesite basalt sintering in the investigated temperature range from 1040 to 1080 °C. However, when the XRD patterns of obtained ceramic materials were compared with the XRD pattern of starting andesite basalt powder the appearance of reddish-brown hematite become apparent due to the sintering procedure conducted in the air.

5. The highest hardness and fracture toughness values of 6.7 GPa and 2.2 MPa√m, respectively, were achieved during the sintering at 1060 °C for 60 min.

Results of the presented study demonstrated that the andesite basalt can be successfully used for the obtainment of high-density ceramics with satisfactory mechanical properties suitable for various industrial applications.

Declarations

Acknowledgments

This work was financially supported by the Ministry of Education, Science, and Technological Development of the Republic of Serbia (Contract No. 451-03-9/2021-14/200017). Authors would also like to acknowledge the help of Dr. Smilja Marković from the Institute of Technical Sciences of The Serbian Academy of Sciences and Arts (SASA), Serbia, during the particle size distribution analysis.

References

1. Morse SA (1980) Basalts and Phase Diagrams: An Introduction to the Quantitative Use of Phase Diagrams in Igneous Petrology. Springer-Verlag, New York (US)
2. Poznyak AI, Levitskii IA, Barantseva SE (2012) Basaltic and granitic rocks as components of ceramic mixes for interior wall tiles. Glas Ceram 69:262–266
3. Kapur S, Sakarya N, Karaman C et al (1995) Micromorphology of Basaltic Ceramics. Brit Ceram Trans 94:33–37
4. Kirsch M, Berger G, Banach U et al (1988) Vitroceramics - A Non-Conventional Kind of Ceramics. Intercer 37:34–38
5. Matović B, Bošković S, Logar M (2003) Preparation of basalt-based glass ceramics. J Serb Chem Soc 68:505–510
6. Čikara D, Todić A, Todić T. Research for possibilities of processing domestic basalt in production of basalt glass. *IMK 14 R&D* 2010, **16**: 1–5. (in Serbian)
7. Wei B, Cao H, Song S (2010) Environmental resistance and mechanical performance of basalt and glass fibers. Mat Sci Eng A – Struct 527:4708–4715
8. Todić A, Čikara D, Todić T et al. Research of toughness particulate composites basis on basalt, polymer and silan. *IMK 14 R&D* 2009, **15**: 25–28. (in Serbian)
9. Khater GA, Abu Safiah MO, Hamzawy EMA (2015) Augite-anorthite glass-ceramics from residues of basalt quarry and ceramic wastes. Process Appl Ceram 9:117–123
10. Matkó S, Keszei S, Csontos I et al (2006) Fire retarded insulating sheets from recycled materials. Macromol Symp 233:217–224
11. Wang MC, Zhang ZG, Li YB (2008) Chemical durability and mechanical properties of alkali-proof basalt fiber and its reinforced epoxy composites. J Reinf Plast Comp 27:393–407
12. Prstić A, Simić R, Andrić L et al (2003) Melting and casting of basalt ore. In *X Balkan Mineral Processing Congress*: *Mineral Processing in 21st Century*. Varna, 893–897

13. Prstić A, Aćimović-Pavlović Z, Andrić L et al (2005) Application of casting materials based on basalt ore in metallurgy and mining industry. In *XI Balkan Mineral Processing Congress*: *Mineral Processing in Sustainable Development*. Tirana, 422–425
14. Beall GH, Rittler HL (1976) Basalt glass ceramics. Am Ceram Soc Bull 55:579–582
15. Pavlović M, Sarvan M, Klisura F et al (2016) Basalt - Raw Material for Production of Aggregate for Modern Road and Rail Shourd. In *4th Conference Maintenace*. Zenica, 175–183
16. Pavlović M, Duricic M, Mumdic A (2015) Basalt Application Prospects for Touristic Facilities Furnishing. In *Conference SED*. Užice, 53–60
17. Čikara D, Todić A, Čikara-Anić D (2010) Possibilities of Production of Wear Resistant Construction Elements by Processing of Serbian Basalt. FME Trans 38:203–207
18. Andric Lj, Acimovic-Pavlovic Z, Trumic M et al (2012) Specific characteristic of coating glazes based on basalt. Mater Des 33:9–13
19. Lima LF, Mantas PQ, Segadães AM et al (2020) Processing and characterization of sinter-crystallized basalt glass-ceramics. J Non-Cryst Solids 538:120019. https://doi.org/10.1016/j.jnoncrysol.2020.120019
20. Lima LF, Zorzi JE, Cruz RCD. Basaltic glass-ceramic: A short review. Bol Soc Esp Ceram V 2020. "in press". https://doi.org/10.1016/j.bsecv.2020.07.005
21. Khater GA, Mahmoud MA (2017) Preparation and characterization of nucleated glass-ceramics based on basaltic rocks. J Aust Ceram Soc 53:433–441
22. Khater GA, Abdel-Motelib A, El Manawi AW et al (2012) Glass-ceramics materials from basaltic rocks and some industrial waste. J Non-Cryst Solids 358:1128–1134
23. Klein JM, da Silva KMS, Titton AP et al (2019) Microstructure and mechanical properties of a nucleant-free basaltic glass-ceramic. Mater Sci Technol 35:544–551
24. Cocić M, Logar M, Matović B et al (2010) Glass-Ceramics Obtained by the Crystallization of Basalt. Sci Sinter 42:383–388
25. Jamshaid H, Mishra R (2016) A green material from rock: basalt fiber – a review. J Text I 107:923–937
26. Albert E, Muntean M, Ianculescu A et al (2009) Special Ceramic Material Based On Basaltic – Andesite For Extreme Environments. Adv Mat Res 59:39–41
27. Matovic B, Maletaskic J, Zagorac J et al (2020) Synthesis and characterization of pyrochlore lanthanide (Pr, Sm) zirconate ceramics. J Eur Ceram Soc 40:2652–2657
28. Evans AG, Charles EA (1976) Fracture toughness determinations by indentation. J Am Ceram Soc 59:371–372
29. Ponton CB, Rawlings RD (1989) Vickers indentation fracture toughness test Part 1: Review of literature and formulation of standardized indentation toughness equations. Mater Sci Tech 5:865–872

30. Ponton CB, Rawlings RD (1989) Vickers indentation fracture toughness test Part 2: Application and critical evaluation of standardized indentation toughness equations. Mater Sci Tech 5:961–976
31. Glandus JC, Rouxel T, Tai Q (1991) Study of the Y–TZP toughness by an indentation method. Ceram Int 17:129–135
32. Karamanov A, Ergul S, Akyildiz M et al (2008) Sinter-crystallization of a glass obtained from basaltic tuffs. J Non Cryst Solids 354:290–295
33. Karamanov A, Maccarini Schabbach L, Karamanova E et al (2014) Sinter-crystallization in air and inert atmospheres of a glass from pre-treated municipal solid waste bottom ashes. J Non-Cryst Solids 389:50–59
34. Karamanov A, Taglieri G, Pelino M (2004) Sintering in nitrogen atmosphere of iron-rich glass-ceramics. J Am Ceram Soc 87:1354–1357
35. Karamanov A (2014) Vitrification and sinter-crystallization of iron-rich industrial wastes. Adv Sci Technol 92:174–183
36. Fomichev SV, Dergacheva NP, Steblevskii AV et al (2011) Production of Ceramic Materials by the Sintering of Ground Basalt. Theor Found Chem En + 45:526–529
37. Karamanov A, Arrizza L, Ergul S (2009) Sintered material from alkaline basaltic tuffs. J Eur Ceram Soc 29:595–601
38. Drobot NF, Noskova OA, Khoroshilov AV et al (2014) Effect of Iron Content on the Sintering of Ground Basalt into Ceramics. Inorg Mater 50:314–319
39. Jeong SS, Nakamura K, Yoshioka S et al (2017) Fracture Toughness of Granite Measured Using Micro to Macro Scale Specimens. Procedia Eng 191:761–767

Figures

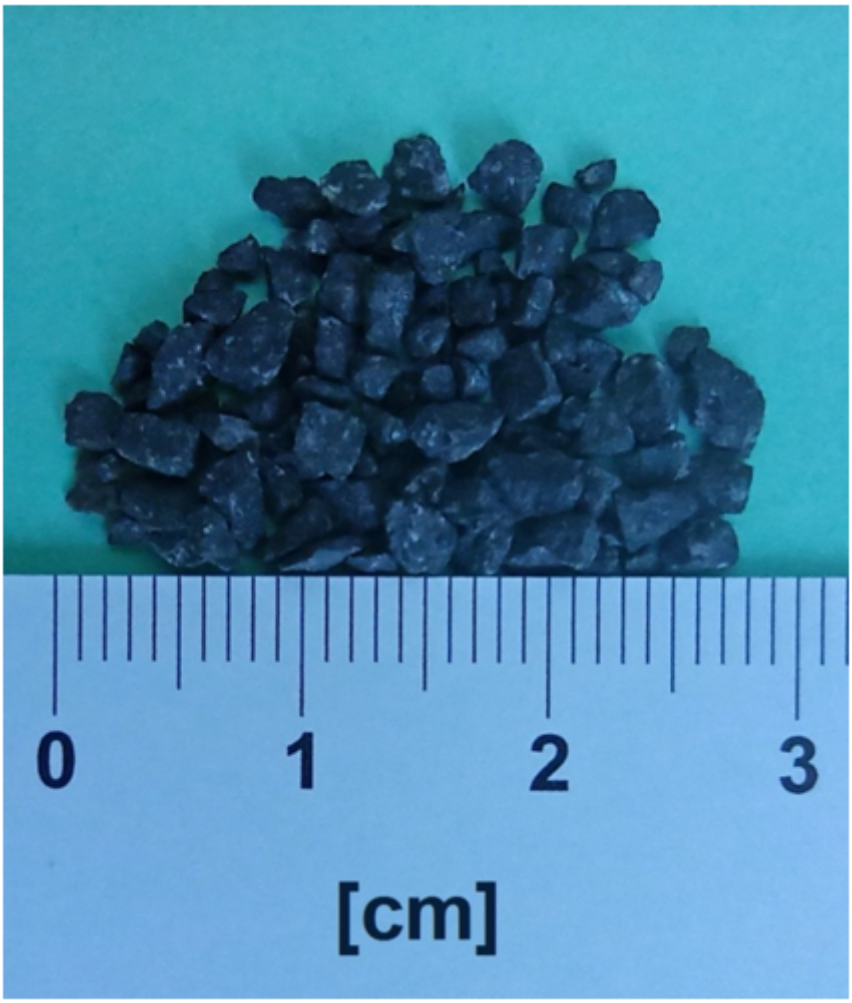

Figure 1

The crushed andesite basalt rock.

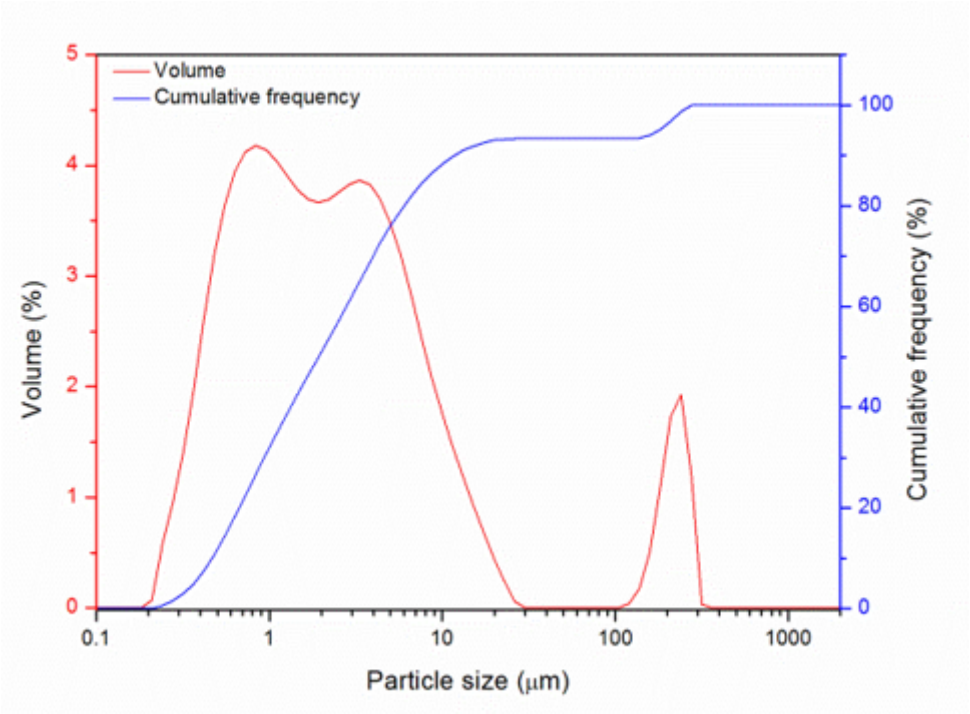

Figure 2

Particle size distribution of the andesite basalt powder obtained after dry milling for 30 min.

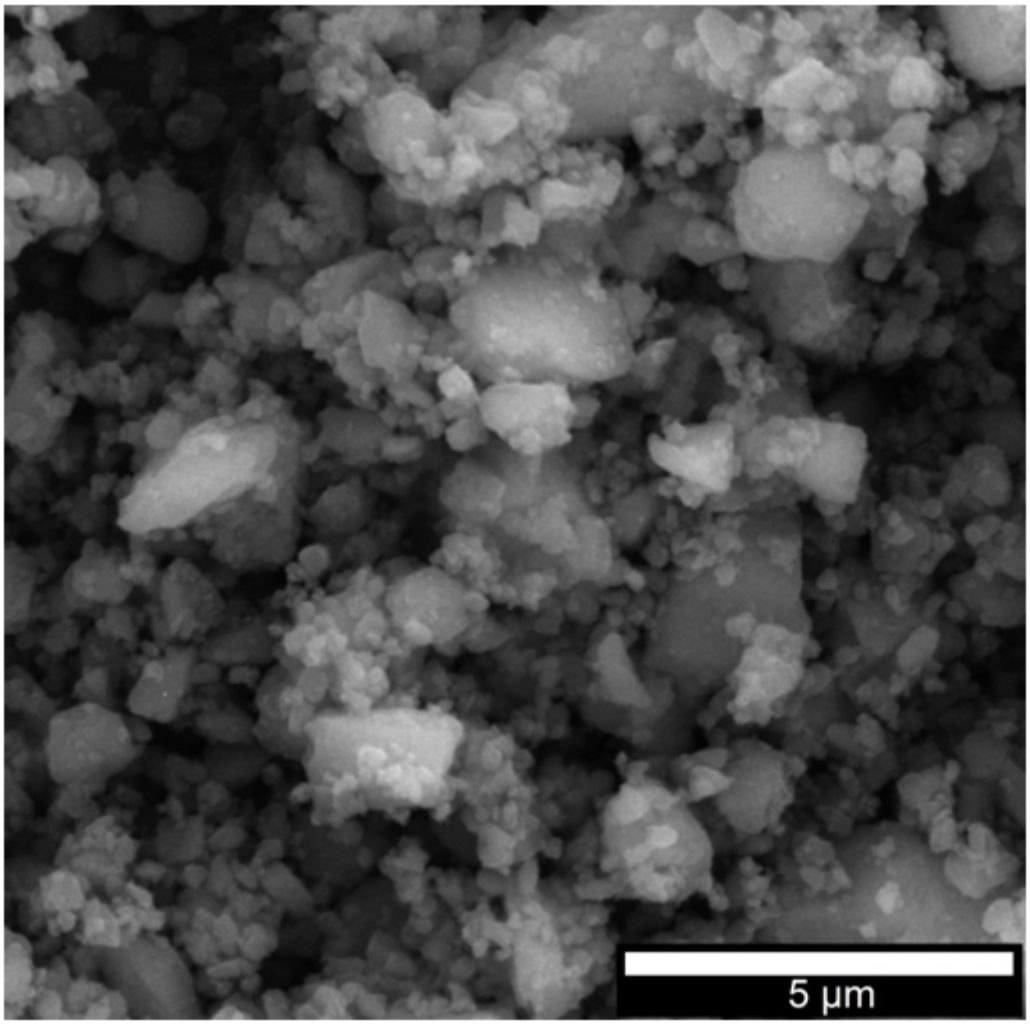

Figure 3

SEM micrograph of the andesite basalt powder obtained after dry milling for 30 min.

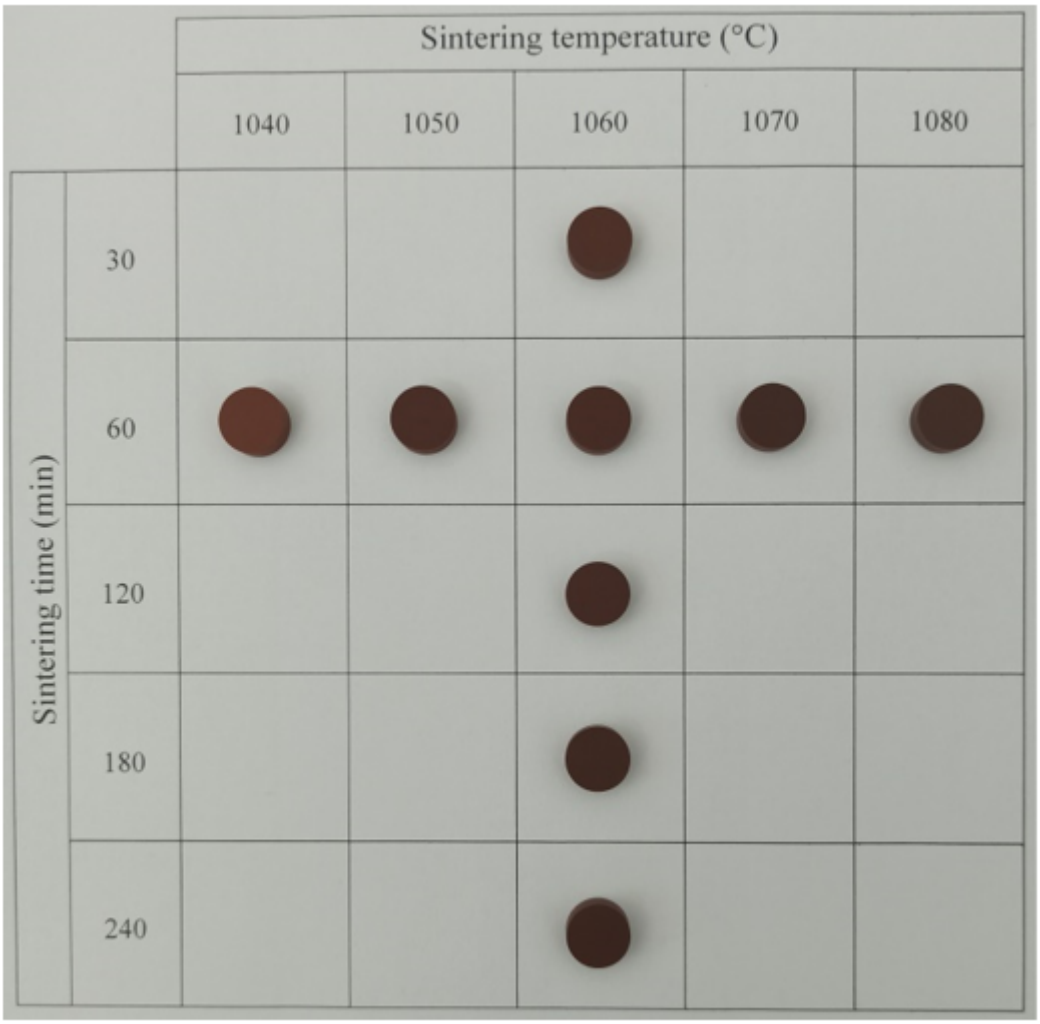

Figure 4

Macrographic overview of the ceramic samples attained during sintering of the andesite basalt powder in the temperature range from 1040 to 1080 °C and in the sintering time range from 30 to 240 min.

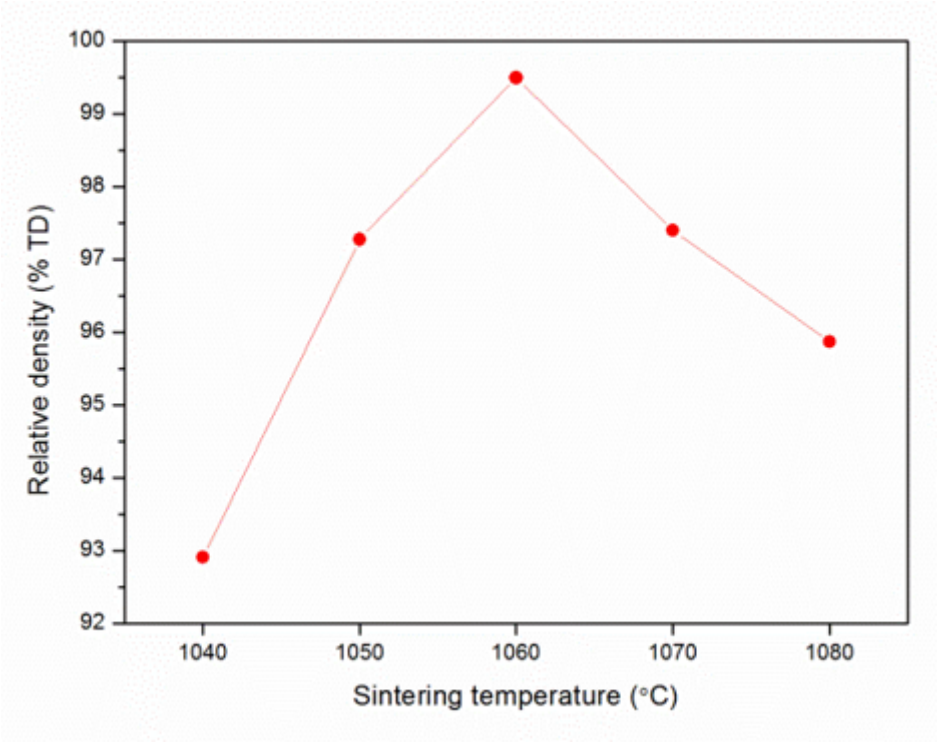

Figure 5

Effect of sintering temperature on the density of ceramic samples obtained during sintering for 60 min.

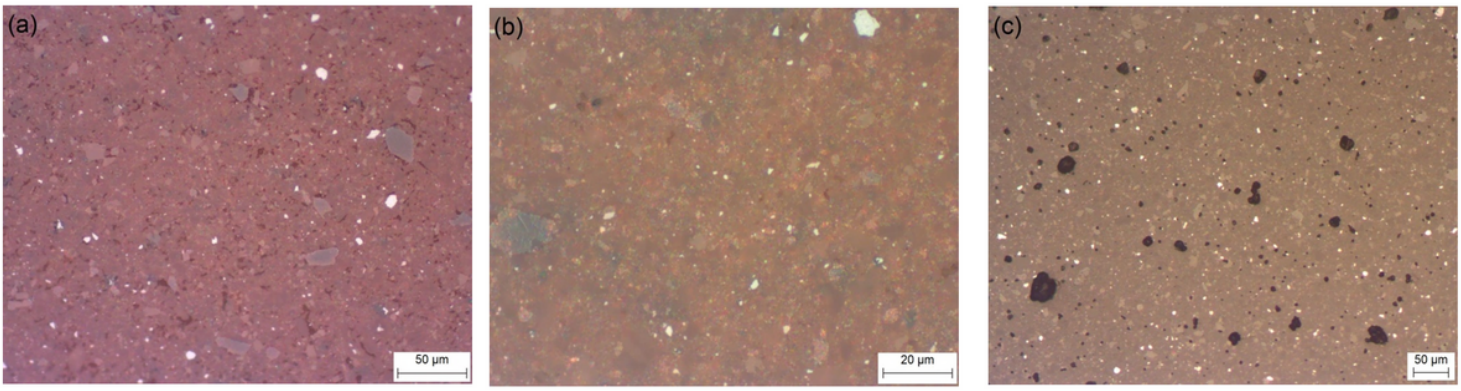

Figure 6

LOM micrographs of the high-density ceramic samples sintered at (a) 1040 °C, (b) 1060 °C, and (c) 1080 °C for 60 min.

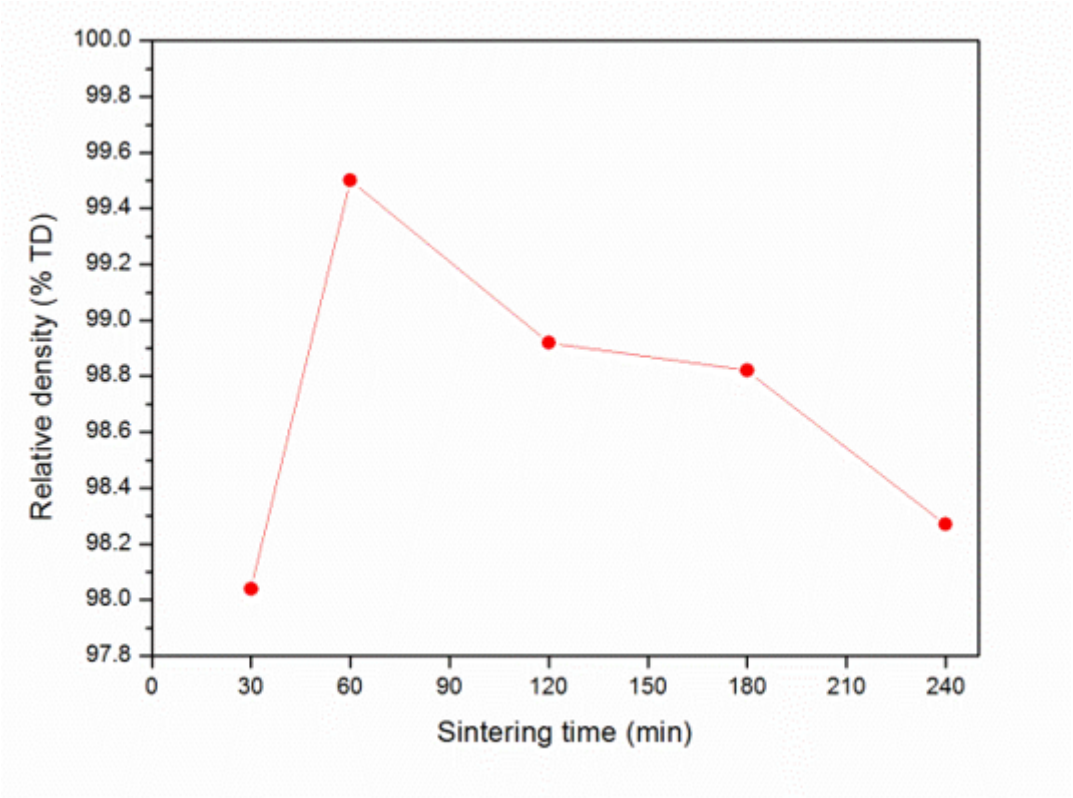

Figure 7

Effect of sintering time on the density of samples obtained after sintering of the andesite basalt powder at 1060 °C.

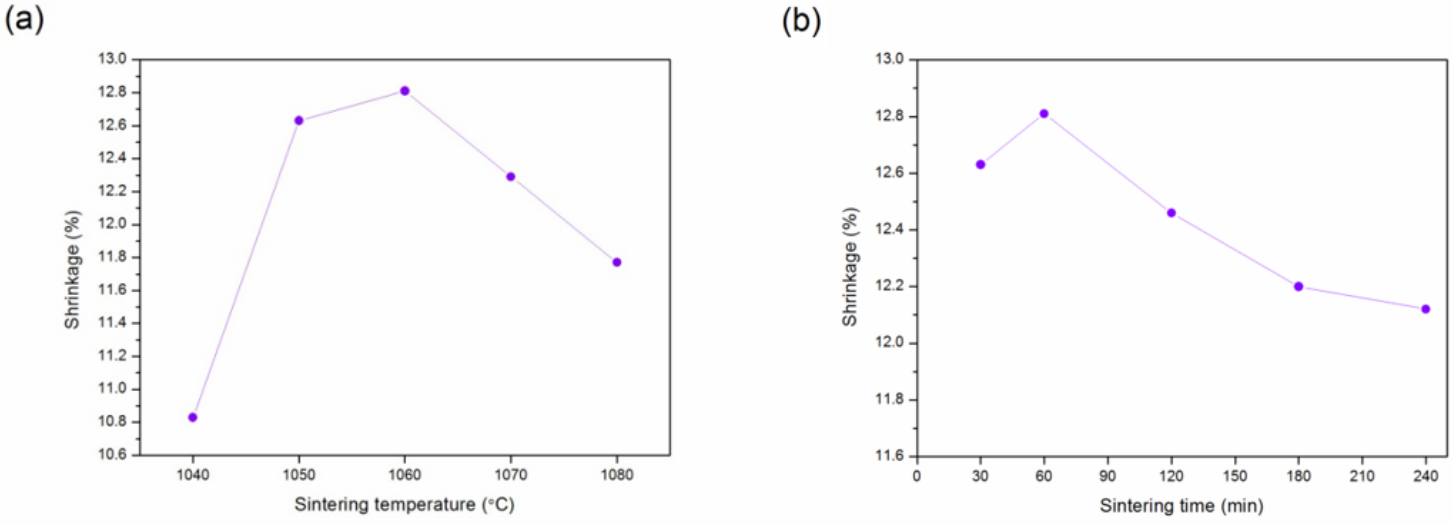

Figure 8

Shrinkage during sintering of the andesite basalt powder at (a) different temperatures for 60 min and (b) 1060 °C for different sintering time.

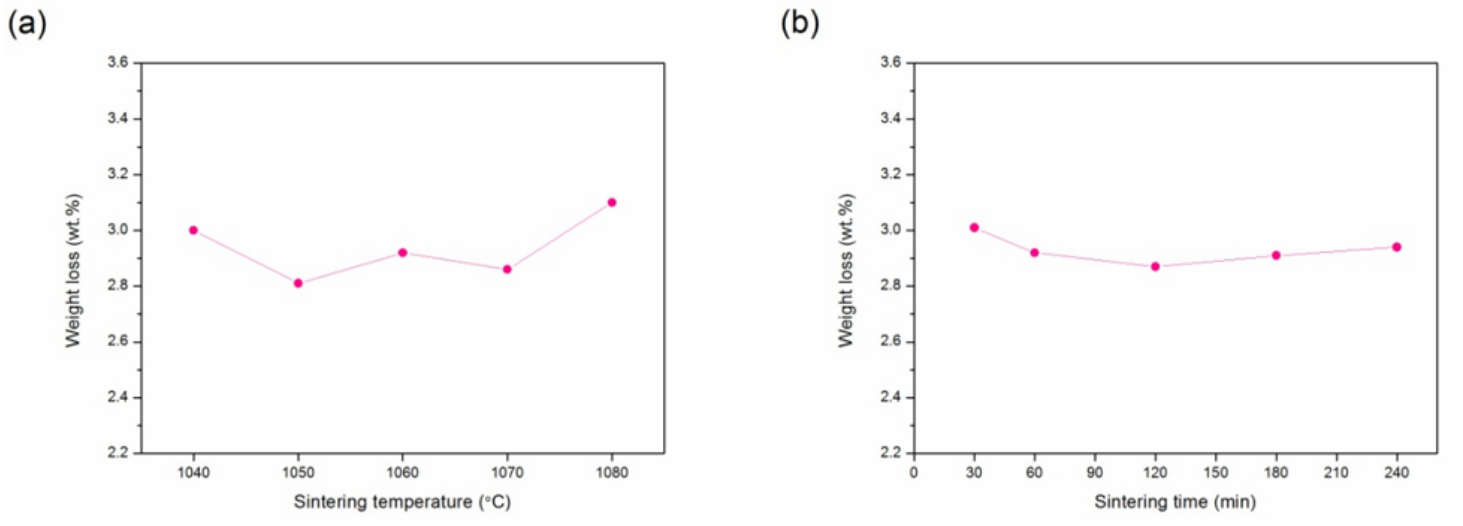

Figure 9

Weight loss during sintering of the andesite basalt powder at (a) different temperatures for 60 min and (b) 1060 °C for different sintering time.

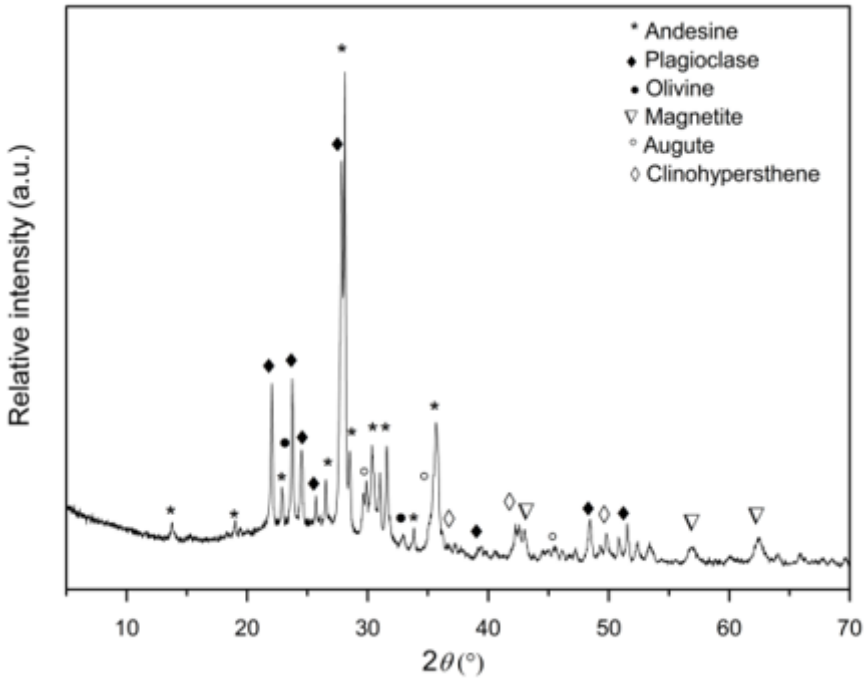

Figure 10

XRD pattern of the starting andesite basalt powder.

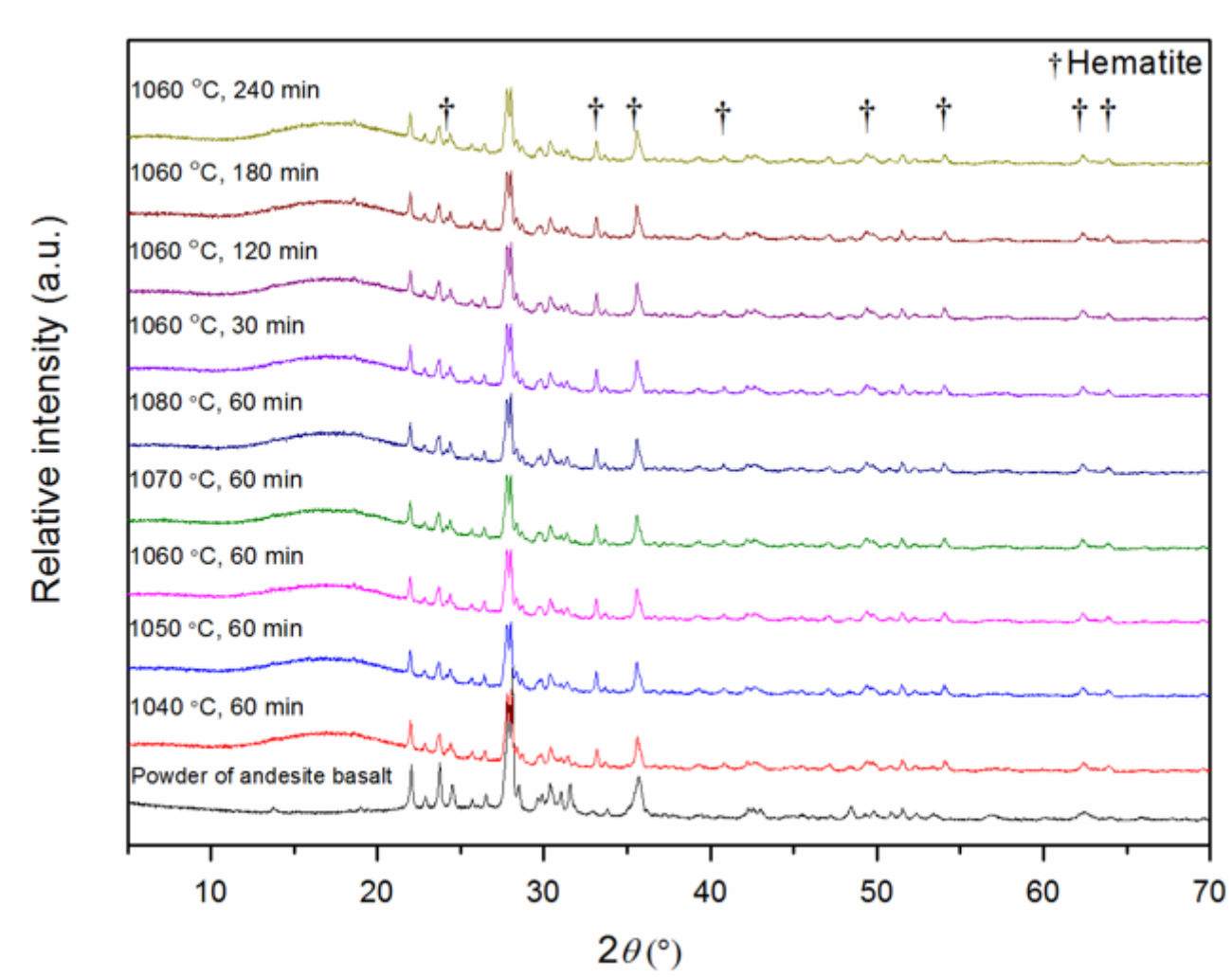

Figure 11

XRD patterns of the andesite basalt powder and ceramic samples attained during sintering under different sintering conditions.

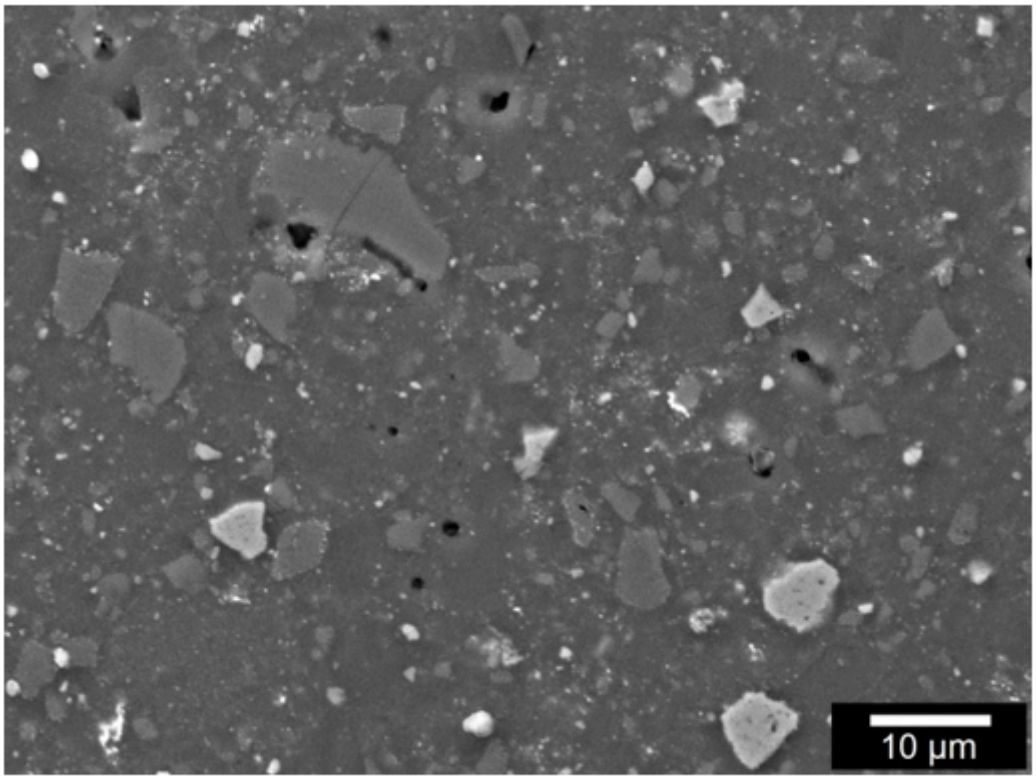

Figure 12

SEM micrograph of the ceramic sample attained during sintering of the andesite basalt powder at 1060 °C for 60 min.

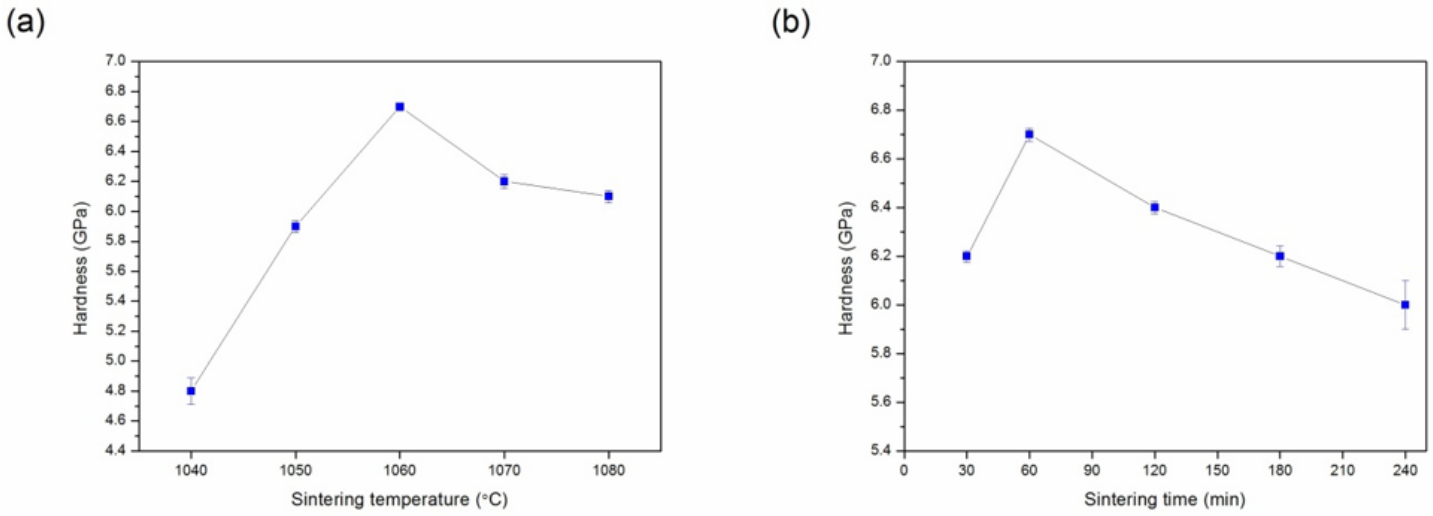

Figure 13

Hardness of ceramic samples attained during sintering of the andesite basalt powder (a) at different temperatures for 60 min and (b) at 1060 °C for different sintering time. Variability of the measured hardness values is presented with standard deviation.

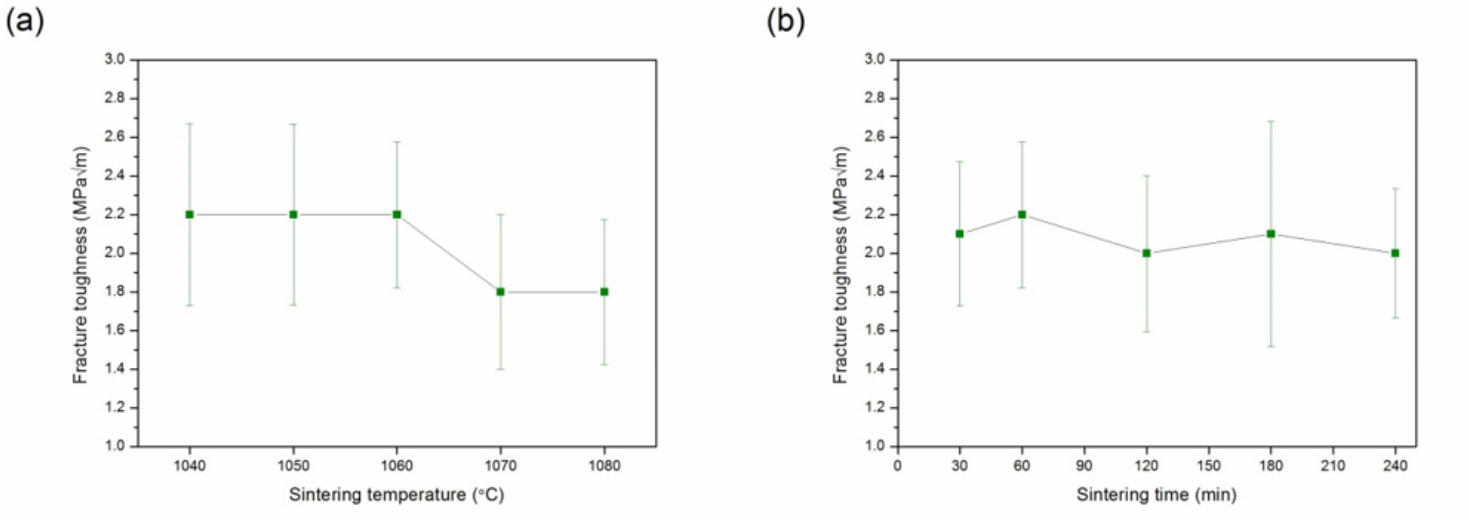

Figure 14

Fracture toughness of ceramic samples attained during sintering of the andesite basalt powder (a) at different temperatures for 60 min and (b) at 1060 °C for different sintering time. Variability of the measured fracture toughness values is presented with standard deviation.

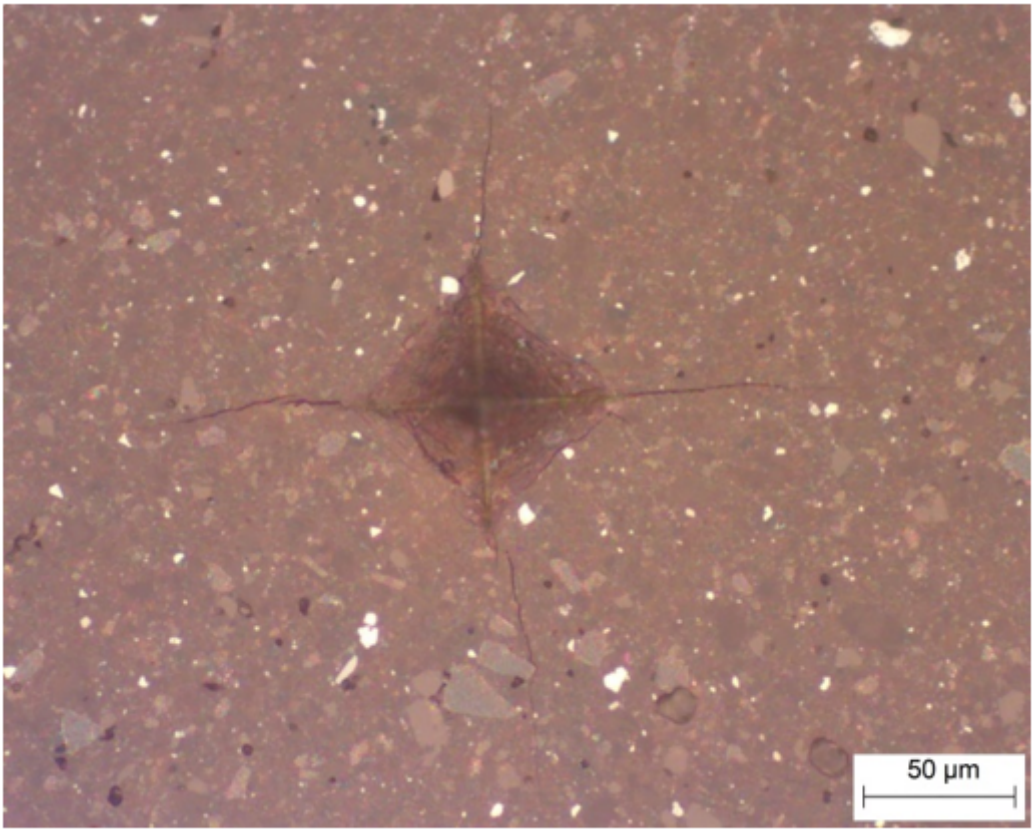

Figure 15

LOM micrograph showing the Vickers indentation impression and cracks formed at the surface of the ceramic sample attained during sintering of the andesite basalt powder at 1060 °C for 60 min.